Task 3 - Large-Scale Testing of Fault Rupture Effects on Bionax Pipe and Pipe Joints

Submitted to:

Jeff Phillips
Western Regional Engineer
IPEX Management, Inc.
20460 Duncan Way
Langley, BC, Canada V3A 7A3
Ph: 604-534-8631
Fax: 604-534-7616
e-mail: Jeff.Phillips@ipexna.com

Submitted by:

School of Civil and Environmental Engineering
Cornell University
Hollister Hall
Ithaca, NY 14853

October, 2013

TABLE OF CONTENTS

LIST OF FIGURES

LIST OF FIGURES (completed)

LIST OF TABLES

1. Introduction

This report is the third in a series of three reports to IPEX Management, Inc. and describes the results of Task 3 – Large-Scale Testing of Fault Rupture Effects on Bionax Pipe and Pipe Joints. The report presents the results of a large-scale test of fault rupture effects on a Bionax pipeline with restrained bell-and-spigot joints performed in the Cornell large-scale test basin in August 2013. All testing was performed at the Cornell University Large Scale Lifelines Testing Facility. IPEX provided all pipe materials and connection fittings. The primary pipe tested was Bionax 6 in. (150mm) CIOD. The joint restraints were Model UFR1559-C-6-I restraints for C909 PVCO, manufactured by the Ford Meter Box Co., Inc.

2. Test Configuration and Procedure

Figure 2.1 is a plan view of the test layout. The pipeline consisted of three pipe segments connected with bell-and-spigot joints and joint restraints. It was buried in the Cornell large-scale test basin in partially saturated sand that was compacted to have an average friction angle of 42º, equivalent in strength to that of a medium dense to dense granular backfill. The depth of burial to top of pipe was 2.5 ft (0.76 m). During the test, the south part of the basin remained stationary, while the north part was displaced to the north and west by large-stroke actuators to cause soil rupture and slip at the interface between the two parts of the test basin. The soil rupture is identical to left lateral strike slip fault rupture, and is also representative of the most severe ground deformation that occurs along the margins of liquefaction-induced lateral spreads and landslides.

A 20-ft-(6.1-m)-long pipe section was placed directly over the fault, with an intersection angle of 50º. The simulated fault rupture caused both tensile and bending strains in the pipeline. The length of the pipeline buried in soil, also mentioned as “test portion,” was approximately 39 ft (11.9 m). Two wooden retaining walls were constructed inside the test basin to support the soil. The test basin was filled with compacted sand, so that the depth of the pipe crown was 30 in. (0.76 m).

The pipe was pressurized with water to approximately 80 psi (552 kPa). The north (movable) portion of the test basin is connected to four MTS hydraulic actuators with load cells controlled by a MTS Flextest GT controller. All actuators were operated in synchronized displacement control. The general test procedure, after all soil placement and instrumentation was installed was:

a) Verify pipe internal pressure,
b) Move the test basin 10 in. (254 mm) at a rate of 2 in./minute (50 mm/minute),

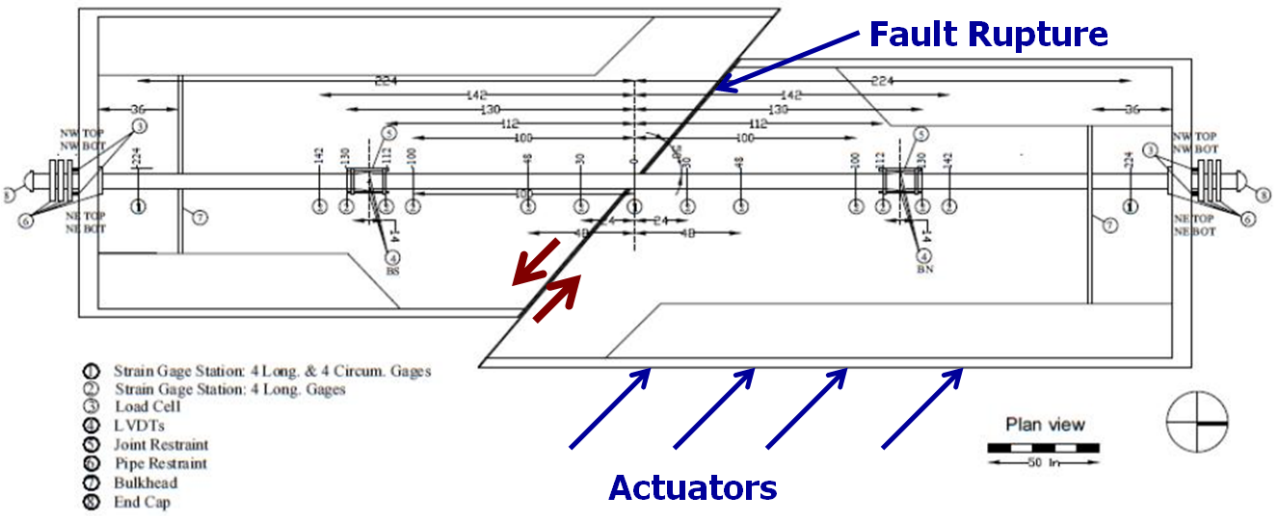

Figure 2.1. Plan View of IPEX Bionax Pressurized Pipe Centered Specimen in Test Basin

c) Verify data collection, and system integrity

e) Begin moving basin again until pipe failure.

At a fault displacement of 12.6 in. (320 mm) there was pipe rupture near the south joint restraint causing the pressure to drop to zero. The test was then stopped.

3. Instrumentation

Figure 2.1, a plan view of the test layout, shows the locations of the instruments along the test pipeline. The instrumentation consisted of strain gages at fifteen locations (gage planes) along the pipeline, load cells at the ends of the pipeline and DCDTs (Direct Current Differential Transformers) to measure joint displacements. To help correlate gage, joint, and load cell locations with the description of measurements in this report, an expanded view of Figure 2.1 is provided in Appendix A.

Seventy-two strain gages were installed in fifteen locations along the pipeline to measure strains and to evaluate axial forces and bending moments. Strain gages were positioned at the crown (C) and invert (I), and at the east (E) and west (W) springlines of the pipe. The strain gage station locations are shown in Figure 2.1. Strain gage stations identified with number 1 consist of eight strain gages, four in the longitudinal direction and 4 around the circumference of the pipe. Strain gage stations identified with number 2 consist of 4 strain gages installed in the longitudinal direction.

Table 3.1 provides the number of strain gage station locations with respect to the fault and joints. Strain gage locations were chosen on the basis of the expected deformed shape and axial behavior of the pipeline as determined from axial pull tests performed at Cornell University as well as the results of finite element analyses of the test, using the code Abaqus 6.11. Strain gage stations 224 and -224, located outside the buried portion of the pipeline, were intended to provide measurements of the end loads. Strain gage stations -48, -24, 0, 24 and 48 are important to determine the deformed shape of the pipeline. Strain gage stations close to the joint restraints, -130,-112, 112 and 130, were placed to assess strain concentration near the restrained joints. Table 3.1 provides locations and coding for the twenty-one gage stations and seven gage planes.

Four DCDTs were placed at each joint to measure the joint pullout and rotation, bell to bell collar relative movement, and bell-to-spigot collar movement. To measure joint pullout and rotation, two DCDTs were mounted on the east and west springlines of the bell. In Figure 3.1 arrows above depict the setup of the springline DCDT. The DCDT sits atop two curved mounting brackets and was fixed to the pipe by a single hose clamp. The DCDT's core was then attached to an angled bracket on the spigot. An identical setup was installed along the other springline of the pipe, and hence the system of DCDTs could measure pullout and rotation.

Figure 3.2 shows a DCDT mounted on the bell with screw-mounted connections to the bell end collar of the restraint to measure bell-to-clamp displacement. Similarly, the bell-to-clamp displacement at the spigot end was measured by mounting a DCDT on the bell, with screw-mounted connections to the spigot end collar of the restraint. Table 3.2 provides the locations and the labeling of the joint DCDTs. Figure 3.3 is an overview of the pipe joint with the restraint. The spigot is inserted into the bell approximately 6 in. (152 mm). After the instrumentation is installed, a protective shielding was then screwed into the restraints. Each shield was mounted to the restraint via twenty four ¼-20 screws (12 on each restraint). Figure 3.4 is an overview of the pipe joint with the protective shielding.

Eight calibrated load cells were positioned at the ends of the test basin. Four load cells were placed between the tension restraint of the pipe and the outer part of the test basin structural steel frame to measure axial loads at the ends of the pipeline during the test. Table 3.3 provides the locations and the labeling of the load cells.

Table 3.1. Strain Gage Locations and Coding System for IPEX Bionax Pressurized Pipe Centered Test

Gage Station	Gages	Distance from Fault	Distance from Closest Joint Center
-224	-224EA-East Springline, Longitudinal -224CA-Crown, Longitudinal -224WA-West Springline, Longitudinal -224IA-Invert, Longitudinal -224EH-East Springline, Circumferential -224CH-Crown, Circumferential -224WH-West Springline, Circumferential -224IH-Invert, Circumferential	224 in. (569 cm) south	104 in. (264 cm) south of south joint
-142	-142EA-East Springline, Longitudinal -142CA-Crown, Longitudinal -142WA-West Springline, Longitudinal -142IA-Invert, Longitudinal	142 in. (356 cm) south	22 in. (56 cm) south of the south joint
-130	-130EA-East Springline, Longitudinal -130CA-Crown, Longitudinal -130WA-West Springline, Longitudinal -130IA-Invert, Longitudinal	130 in. (330 cm) south	10 in. south (25 cm) of the south joint
-112	-112EA-East Springline, Longitudinal -112CA-Crown, Longitudinal -112WA-West Springline, Longitudinal -112IA-Invert, Longitudinal	112 in. (284 cm) south	8 in. (20 cm) north of the south joint
-100	-100EA-East Springline, Longitudinal -100CA-Crown, Longitudinal -100WA-West Springline, Longitudinal -100IA-Invert, Longitudinal	100 in. (254 cm) south	20 in. (51 cm) north of the south joint
-48	-48EA-East Springline, Longitudinal -48CA-Crown, Longitudinal -48WA-West Springline, Longitudinal -48IA-Invert, Longitudinal	48 in. (122 cm) south	72 in. (183 cm) north of the south joint
-24	-24EA-East Springline, Longitudinal -24CA-Crown, Longitudinal -24WA-West Springline, Longitudinal -24IA-Invert, Longitudinal	24 in.(61 cm) south	96 in. (244 cm) north of the south joint

Table 3.1. Strain Gage Locations and Coding System for IPEX Bionax Pressurized Pipe Centered Test (completed)

Gage Station	Gages	Distance from Fault	Distance from Closest Joint Center
0	0EA-East Springline, Longitudinal 0CA-Crown, Longitudinal 0WA-West Springline, Longitudinal 0IA-Invert, Longitudinal 0EH-East Springline, Circumferential 0CH-Crown, Circumferential 0WH-West Springline, Circumferential 0IH-Invert, Circumferential	0	120 in. (305 cm)north of the south joint
24	24EA-East Springline, Longitudinal 24CA-Crown, Longitudinal 24WA-West Springline, Longitudinal 24IA-Invert, Longitudinal	24 in. (61 cm) north	96 in. (244 cm) south of the north joint
48	48EA-East Springline, Longitudinal 48CA-Crown, Longitudinal 48WA-West Springline, Longitudinal 48IA-Invert, Longitudinal	48 in. (122 cm) north	72 in. (183 cm) south of the north joint
100	100EA-East Springline, Longitudinal 100CA-Crown, Longitudinal 100WA-West Springline, Longitudinal 100IA-Invert, Longitudinal	100 in. (254 cm) north	20 in. (51 cm) south of the north joint
112	112EA-East Springline, Longitudinal 112CA-Crown, Longitudinal 112WA-West Springline, Longitudinal 112IA-Invert, Longitudinal	112 in. (284 cm) north	8 in. (20 cm) south of the north joint
130	130EA-East Springline, Longitudinal 130CA-Crown, Longitudinal 130WA-West Springline, Longitudinal 130IA-Invert, Longitudinal	130 in. (330 cm) north	10 in. (25 cm) north of the north joint
142	142EA-East Springline, Longitudinal 142CA-Crown, Longitudinal 142WA-West Springline, Longitudinal 142IA-Invert, Longitudinal	142 in. (356 cm) north	22 in.(56 cm) north of the north joint
224	224EA-East Springline, Longitudinal 224CA-Crown, Longitudinal 224WA-West Springline, Longitudinal 224IA-Invert, Longitudinal 224EH-East Springline, Circumferential 224CH-Crown, Circumferential 224WH-West Springline, Circumferential 224IH-Invert, Circumferential	224 in. (569 cm) north	104 in. (264 cm) north of the north joint

Table 3.2. DCDT Locations and Labeling for IPEX Bionax Pressurized Pipe Centered Test

Location	Displacement Measurement Device	Type and Stroke
South Joint	SESL – East Springline	DCDT ± 2 in.
	SBBR – Bell to Bell Restraint	DCDT ± 2 in.
	SBSR – Bell to Spigot Restraint	DCDT ± 2 in.
	SWSL – West Springline	DCDT ± 2 in.
North Joint	NESL – East Springline	DCDT ± 2 in.
	NBBR – Bell to Bell Restraint	DCDT ± 2 in.
	NBSR – Bell to Spigot Restraint	DCDT ± 2 in.
	NWSL – West Springline	DCDT ± 2 in.

Table 3.3. Load Cell Locations and Labeling for IPEX Bionax Pressurized Pipe Centered Test

Location	Load Cell
South End	SW Top – Outer, West, Top
	SE Top – Outer, East, Top
	SW Bot – Outer, West, Bottom
	SE Bot – Outer, East, Bottom
North End	NW Top – Outer, West, Top
	NE Top – Outer, East, Top
	NW Bot – Outer, West, Bottom
	NE Bot – Outer, East, Bottom

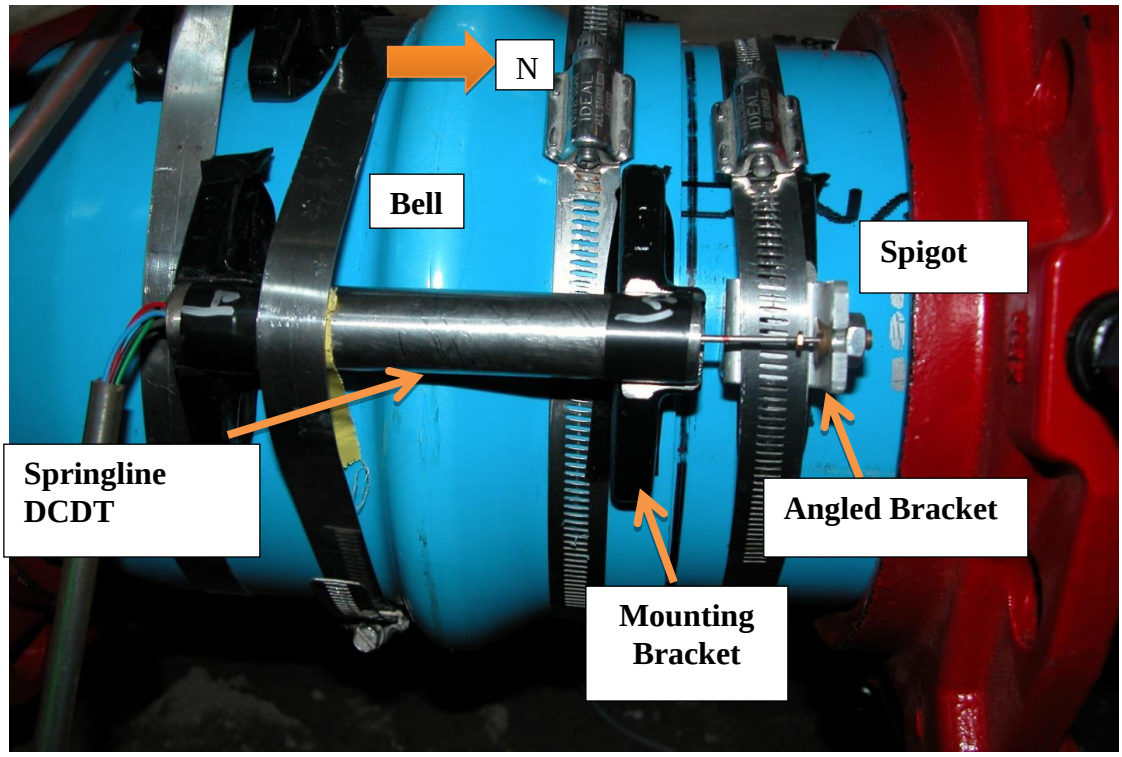

Figure 3.1. Springline DCDT

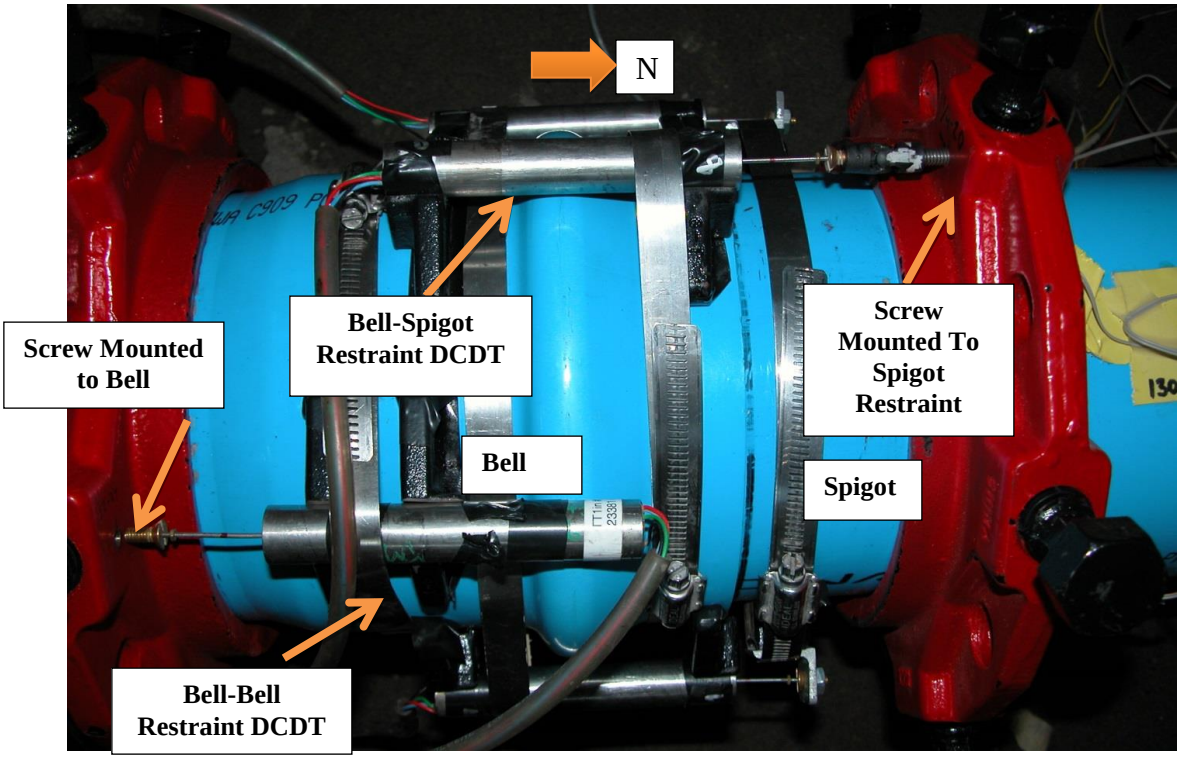

Figure 3.2. DCDTs to Measure the Bell-Bell Restraint and Bell-Spigot Restraint Displacements

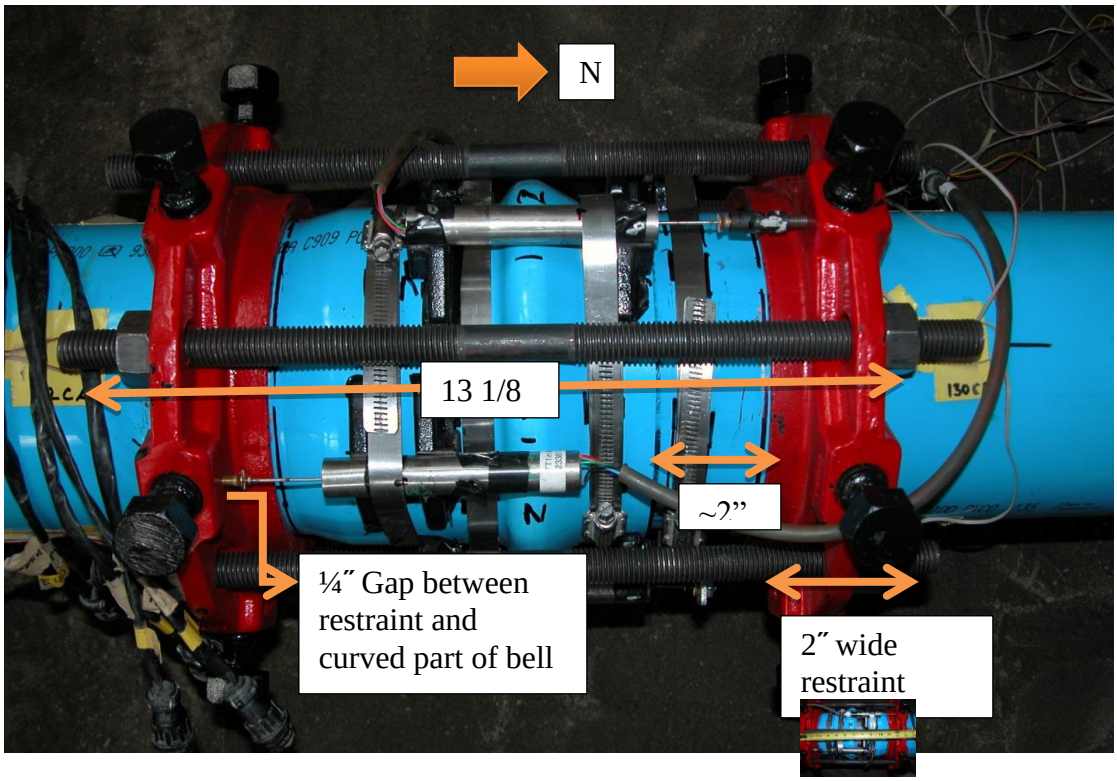

Figure 3.3. Overview of the Joint Restraint

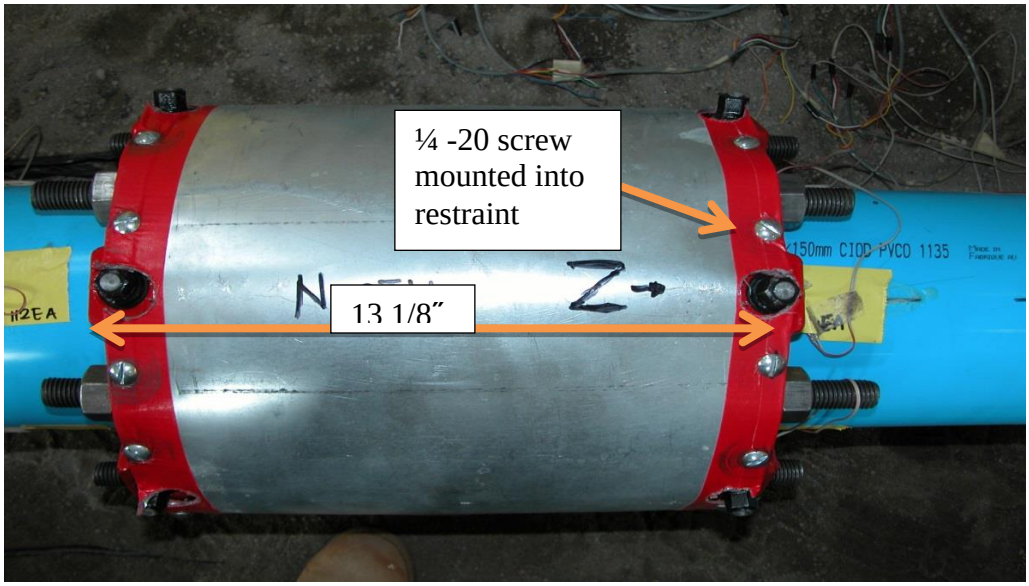

Figure 3.4. Overview of the Joint Restraint with the Protective Shielding

4. Soil Preparation

The soil used during the test was crushed, washed, glacio-fluvial sand produced by RMS Gravel consisting of particles mostly passing the ¼ in. (6.25 mm) sieve. Figure 4.1 is a grain size distribution of the RMS graded sand. Eight in. (203.2 mm) of compacted sand was placed in the test basin, followed by the pipe sections, followed by approximately 8-in.-thick (203-mm) lifts until there was 30 in. (762 mm) cover of compacted sand above the pipe crown. Every layer was compacted to the same extent and moistened with water in a similar way to achieve uniformity. Dry density measurements were taken for each layer using a Troxler Model 3440 densitometer. Moisture content measurements were obtained using both soil samples and the densitometer at the same locations. The target value of dry density was γ_{dry} = 106 pcf (16.7 kN/m^3) and the target value of moisture content was w = 4.0 %, corresponding to an angle of shearing resistance (friction angle) of the sand of approximately 42º.

Eight measurements of dry unit weight and moisture content were made for each soil lift. Figure 4.2 shows the approximate location of each measurement location. There were four measurement positions in the north portion of the test basin and four in the south portion. Table 4.1 lists the adjusted dry unit weights. Table 4.2 provides the moisture contents. The soil dry unit weights were evaluated using single-factor analysis of variance (ANOVA) to make comparisons among the data. Comparisons were made to determine if the dry unit weights for each lift, as measured at eight locations per lift, could be considered equal. Each lift was compared with each other lift, and evaluations of the variations were made. The evaluations indicated that in side-by-side comparisons all lifts could be considered equal with 95% confidence. The global average dry unit weight was 105.9 lb/ft^3 (16.4 kN/m^3) with a standard deviation of 1.4 lb/ft^3 (0.21 kN/m^3). The global average moisture content was 4.0% with a standard deviation of 0.4%.

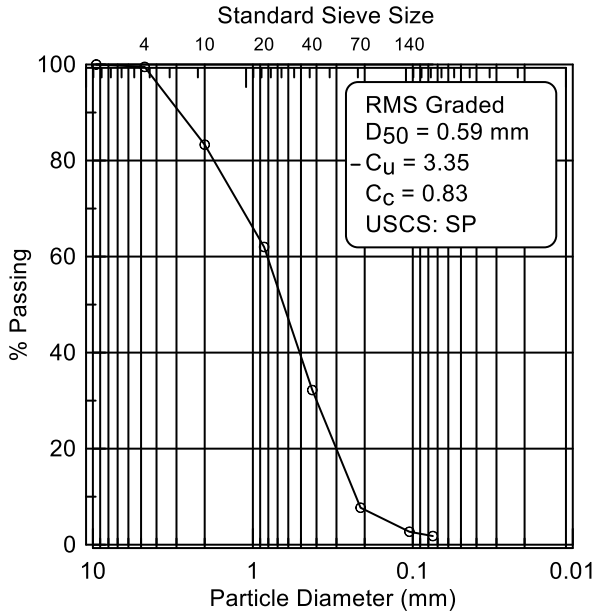

Figure 4.1. Particle Size Distribution of RMS Graded Sand

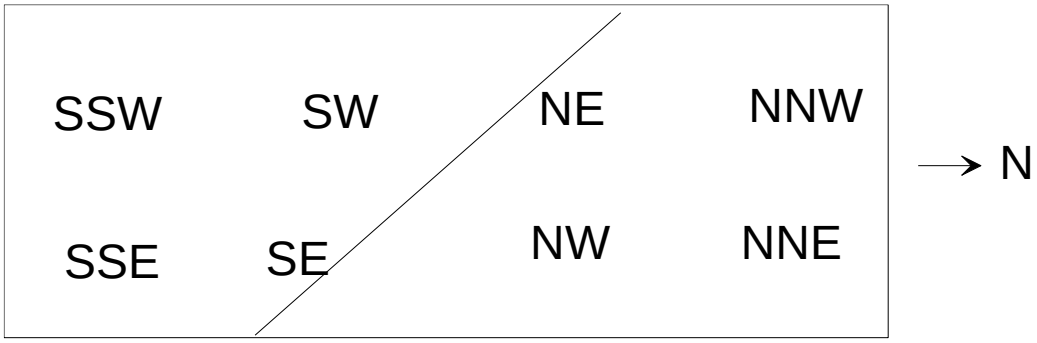

Figure 4.2. Plan View of Locations for Compaction Measurements

Table 4.1. Adjusted Dry Unit Weights for IPEX Bionax Pressurized Pipe Centered Test

	Adjusted Dry Unit Weights (lb/ft^3)				
Location	Lift 1	Lift 2	Lift 3	Lift 4	Lift 5
NNW	103.7	105.2	105.8	104.7	107.4
NW	105.7	107.0	105.9	106.4	105.4
SSW	105.6	105.0	106.0	104.9	104.6
SW	104.4	103.6	106.2	106.3	108.7
SE	105.7	105.3	105.6	106.3	107.5
SSE	103.4	106.9	106.4	107.2	105.8
NE	105.5	107.6	107.6	104.1	108.4
NNE	103.2	105.9	106.3	107.8	107.9
Avg	104.6	105.8	106.2	106.0	107.0
Stdev	1.02	1.24	0.56	1.19	1.41
Global Avg					105.9
Global Stdev					1.37

1 lb/ft^3 = 0.1571 kN/m^3

Table 4.2. Moisture Tin Water Content Data for IPEX Bionax Pressurized Pipe Centered Test

	Moisture Tin Water Content, w (%)				
Location	Lift 1	Lift 2	Lift 3	Lift 4	Lift 5
NNW	4.38	3.71	3.66	4.54	3.76
NW	4.66	3.58	4.68	4.24	3.96
SSW	3.74	4.15	4.44	3.63	4.32
SW	4.09	3.91	3.88	4.31	3.34
SE	3.90	3.99	4.49	3.85	3.70
SSE	3.67	3.99	4.05	3.86	3.78
NE	4.80	3.79	3.48	4.21	4.02
NNE	4.05	3.85	3.27	3.86	4.27
Avg.	4.16	3.87	4.00	4.06	3.89
Stdev	0.39	0.17	0.48	0.29	0.30
Global Avg.					4.02
Global Stdev.					0.36

5. Test Basin Movements

Four actuators are connected between the movable portion of the test basin and the modular reaction wall in the laboratory. From south to north, the actuators are called short-stroke actuator 1 (SSA1), short-stroke actuator 2 (SSA2), long-stroke actuator 1 (LSA1), and long-stroke actuator 2. (LSA2). Each SSA actuator has a displacement range of ± 2 ft (0.61 m) [4 ft (1.22 m) total stroke] and load capacity of 100 kips (445 kN) tension and 145 kips (649 kN) compression. Each LSA actuator has a displacement range of ± 3 ft (0.91 m) [6 ft (1.83 m) total stroke] and load capacity of 63 kips (295 kN) tension and 110 kips (498 kN) compression.

Figure 5.1 shows the displacement of long-stroke actuator 1 (LSA1) versus time. All actuators are synchronized to move at exactly the same rate and displacement, so only LSA1 is shown.

6. Pipe Internal Pressure

The pipe was initially pressurized to 80 psi (552 kPa) before any basin movement. Each movement of the basin caused the pipe to increase slightly in overall length, causing the pressure to fluctuate slightly (a few psi). Figure 6.1 shows the pipe internal pressure vs. fault displacement. At a fault displacement of roughly 12.6 in. (320 mm) there was a sudden loss of pressure in the pipe. At this point the test was stopped and the water drained from the pipe.

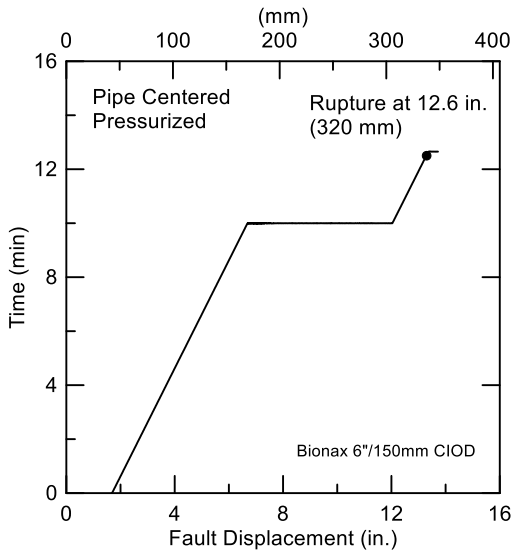

Figure 5.1 Fault Movement vs. Time

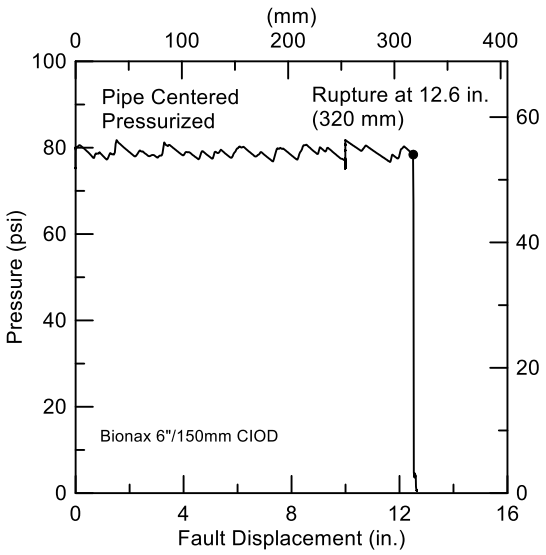

Figure 6.1. Internal Pipe Pressure vs. Fault Displacement

7. Strain Gage Measurements

The distribution of strain gages was symmetrical about the center of the pipe section, which was in turn centered on the fault. The data are presented as the "south" gage sets and "north" gage sets, each at the same distance from the fault. Lateral bending was measured by springline gages on opposite sides of the pipe. The east and west springline gages, orientated in the axial direction, measure axial strain due to a combination of axial force and bending moment. When the strains measured at opposite springlines are the same or nearly the same, the measurements indicate a response only to axial forces. When the springline strains are not similar, it indicates lateral bending.

Figures 7.1 and 7.2 show the axial and hoop pipe strains, respectively, at the crown, invert, east springline, and west springline measured at the -224 in. (-569 cm) gage plane. This plane was outside the soil at the south end of the test basin. Figures 7.3 and 7.4 show the axial and hoop pipe strains, respectively, at the crown, invert, east springline, and west springline measured at the 224 in. (569 cm) gage plane. This plane was outside the soil at the north end of the test basin. The strains at both the south and north stations are in excellent agreement, and indicate symmetry at these gage planes. Neither of the gage planes indicated lateral bending at these locations outside the soil.

Figures 7.5 and 7.6 show the axial strains at 142 in (356 cm) south and north of the fault, respectively. The strains at the crown, invert, and east and west springlines are all in very good agreement and also indicate essentially no lateral pipe bending at these locations.

Figures 7.7 and 7.8 show the axial strains at 130 in. (330 cm) south and north of the fault, respectively. There are differences between strains at the crown, invert, and east and west springlines south of the fault that show increasing levels of bending until failure at the south joint. The strains at the gage locations 130 in. (330 cm) north of the fault are in relatively close agreement.

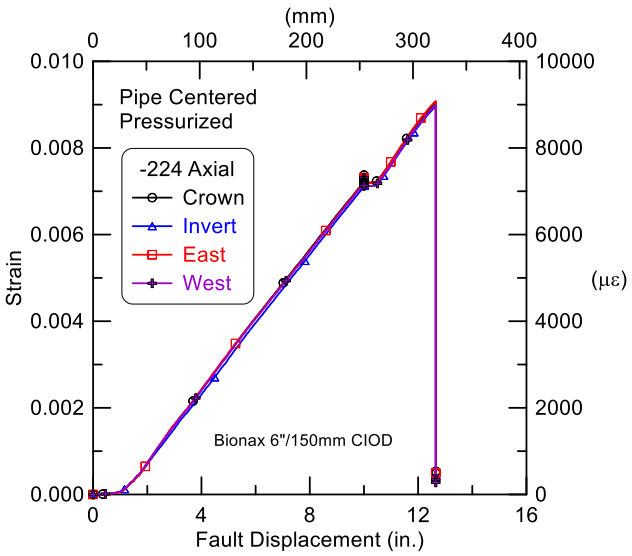

Figure 7.1. Axial Strain vs. Fault Displacement 224 in. (569 cm) South of Fault

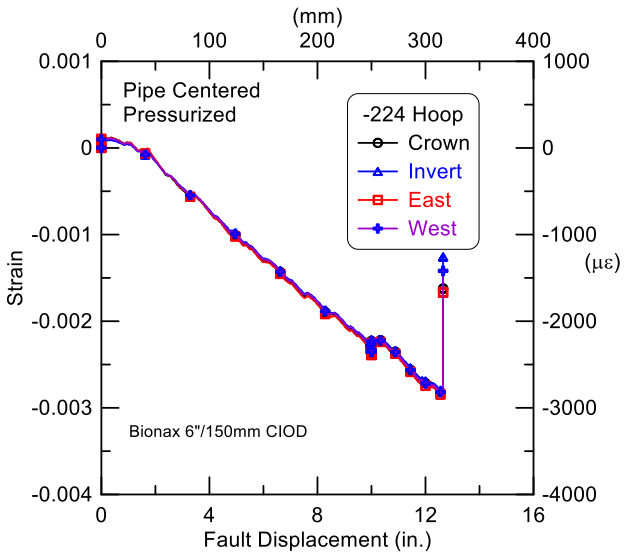

Figure 7.2. Hoop Strain vs. Fault Displacement 224 in. (569 cm) South of Fault

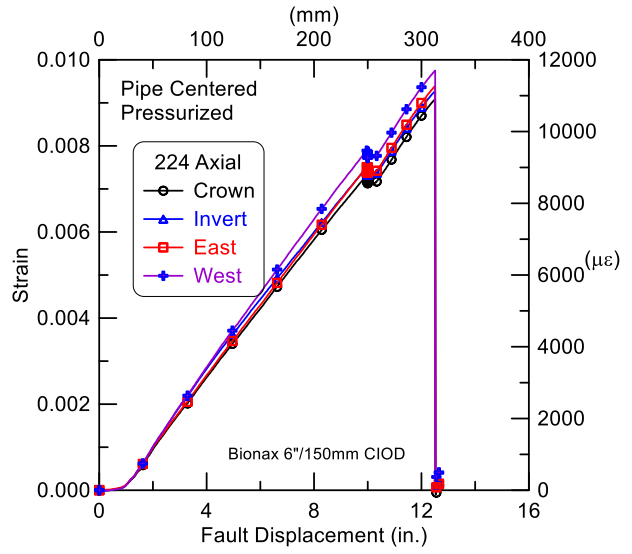

Figure 7.3. Axial Strain vs. Fault Displacement 224 in. (569 cm) North of Fault

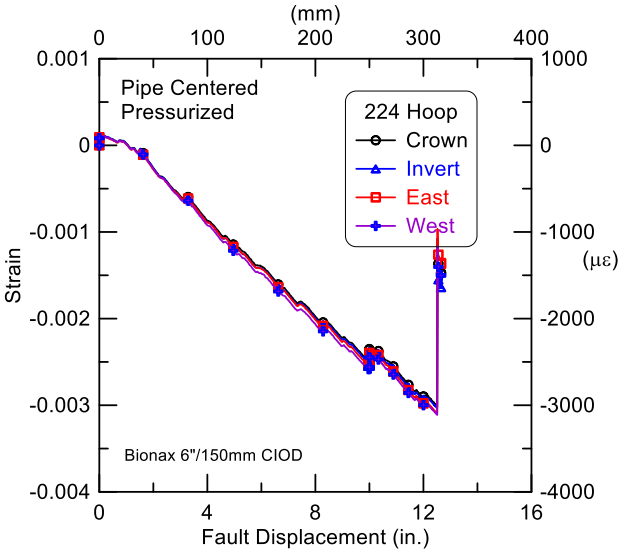

Figure 7.4. Hoop Strain vs. Fault Displacement 224 in. (569 cm) North of Fault

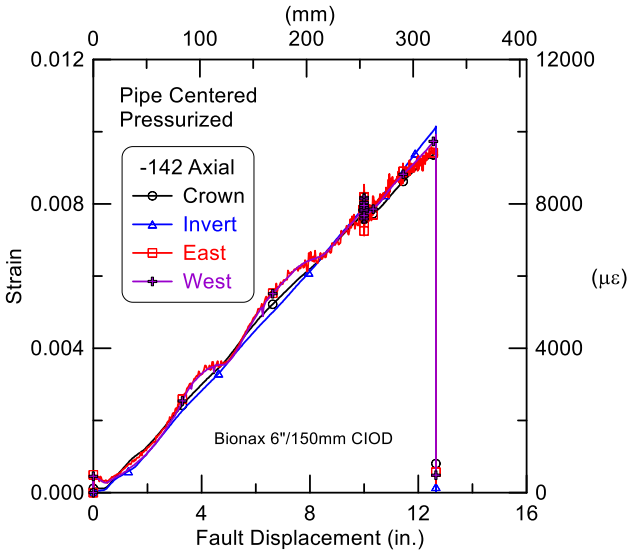

Figure 7.5. Axial Strain vs. Fault Displacement 142 in. (356 cm) South of Fault

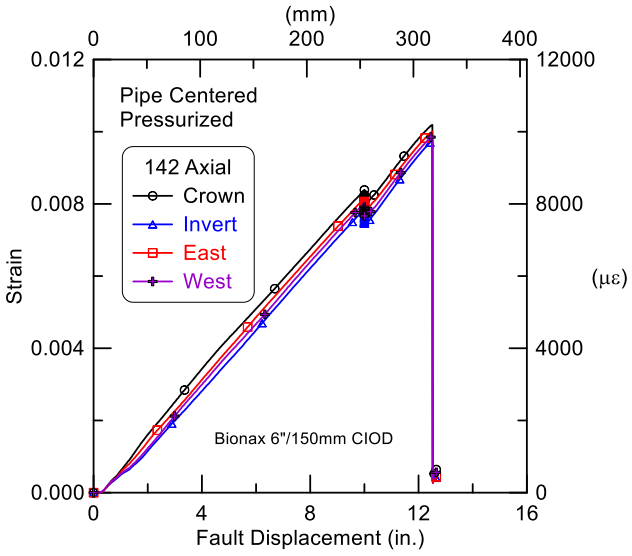

Figure 7.6. Axial Strain vs. Fault Displacement 142 in. (356 cm) North of Fault

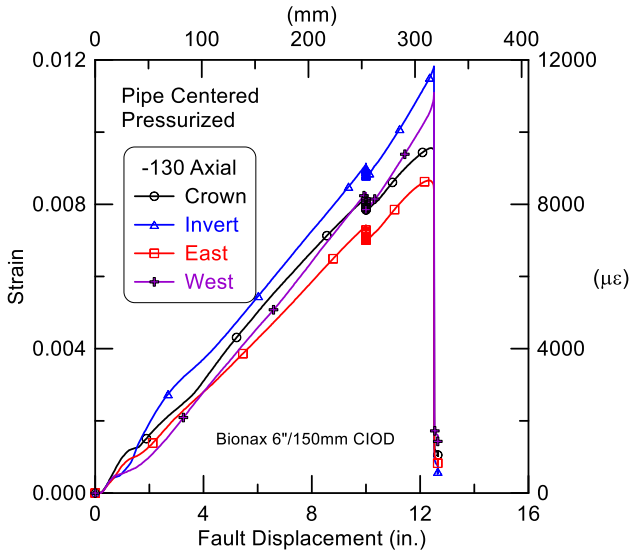

Figure 7.7. Axial Strain vs. Fault Displacement 130 in. (330 cm) South of Fault

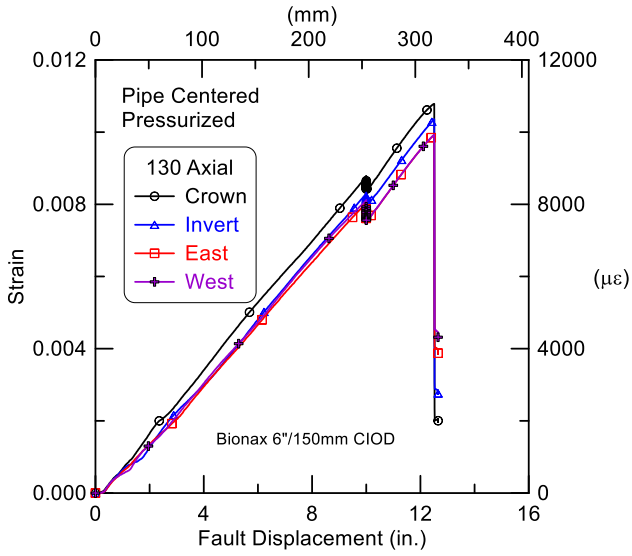

Figure 7.8. Axial Strain vs. Fault Displacement 130 in. (330 cm) North of Fault

Figures 7.9 and 7.10 show the axial strains at 112 in. (284 cm) south and north of the fault, respectively. The strains at the invert and east springline at the gage plane south of the fault did not function properly. The crown and west springlines gages 112 in. (284 cm) south of the fault are in good agreement. All gages at this gage plane north of the fault agree well, and little lateral bending is indicated.

Figures 7.11 and 7.12 show the axial strains at 100 in. (254 cm) south and north of the fault, respectively. The strains at these gage planes both south and north of the fault are all quite similar. There is little to no bending strain at these gage planes.

Figures 7.13 and 7.14 show the measured axial strains at a distance of 48 in. (122 cm) south and north of the fault, respectively. At these locations relatively large bending strains were measured. Note that in Figure 7.13 the east springline strains are much larger than the west springline strains south of the fault, whereas in Figure 7.14 the west springlines strains are much larger than the east springline strains north of the fault. The sign convention for bending strains is such that positive strains reflect how the pipe would be expected to deform. This indicates that the direction of lateral bending is positive (if using a negative right-hand rule) to the west on the north side of the fault. This is consistent with the north portion of the test basin being pushed to the west.

At a distance of 24 in. (61 cm) south and north of the fault, bending strains clearly are present. This is shown in Figures 7.15 and 7.16, south and north of the fault, respectively. Again, Figure 7.15 the east springline strains are much larger than the west springline strains south of the fault, whereas in Figure 7.16 the west springlines strains are much larger than the east springline strains north of the fault.

Figure 7.17 shows the measured axial strains at the fault. Here, there are bending strains but they are considerably smaller than those at 24 and 48 in. (122 and 61 cm) south and north of the fault.

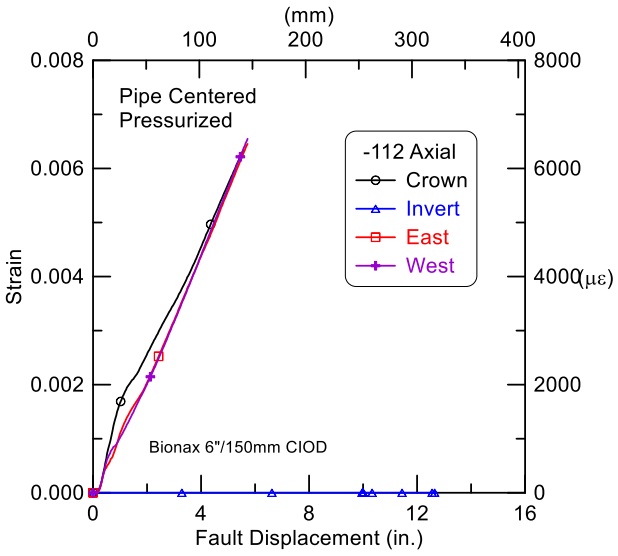

Figure 7.9. Axial Strain vs. Fault Displacement 112 in. (284 cm) South of Fault

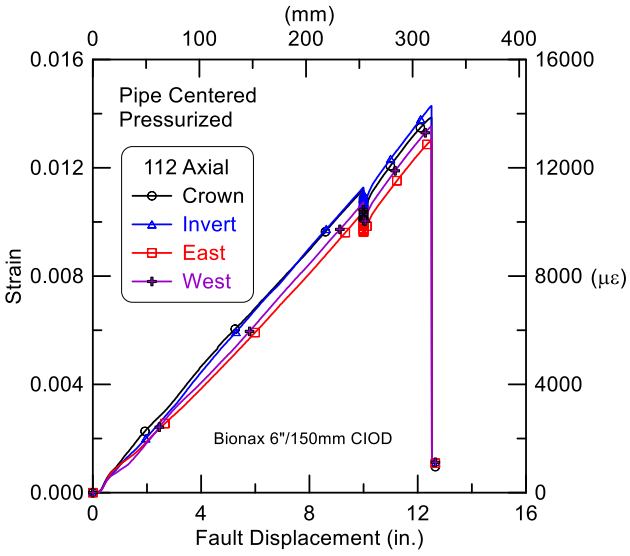

Figure 7.10. Axial Strain vs. Fault Displacement 112 in. (284 cm) North of Fault

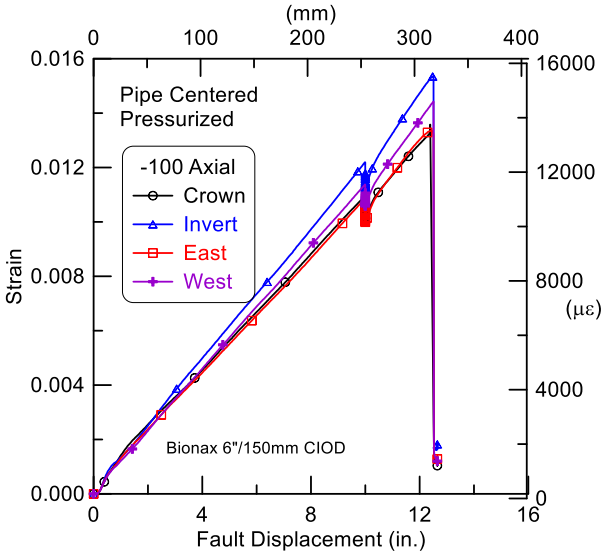

Figure 7.11. Axial Strain vs. Fault Displacement 100 in. (254 cm) South of Fault

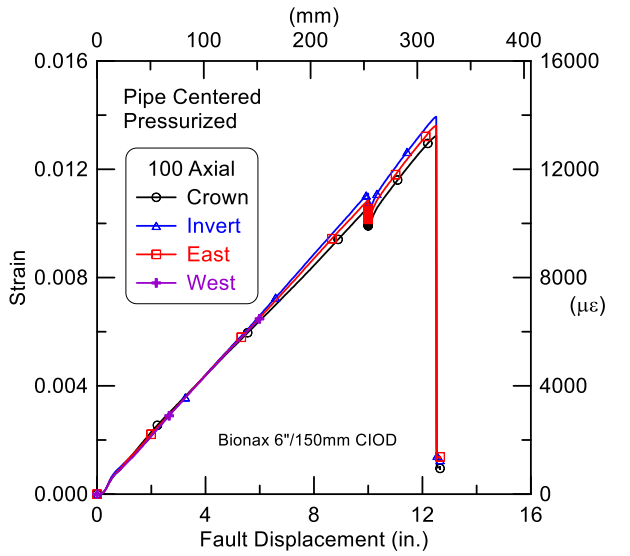

Figure 7.12. Axial Strain vs. Fault Displacement 100 in. (254 cm) North of Fault

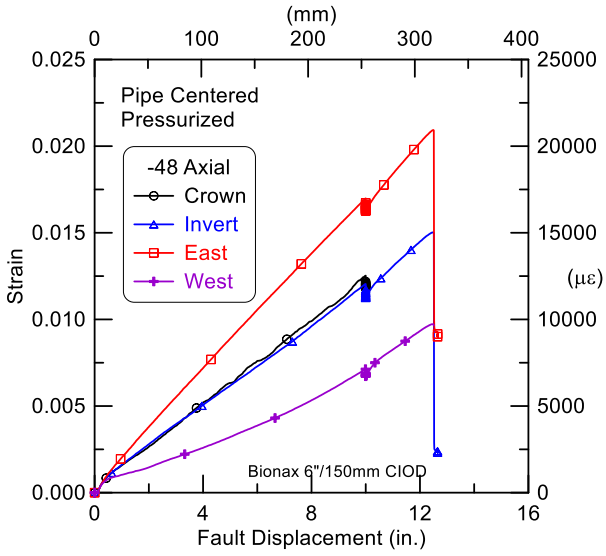

Figure 7.13. Axial Strain vs. Fault Displacement 48 in. (122 cm) South of Fault

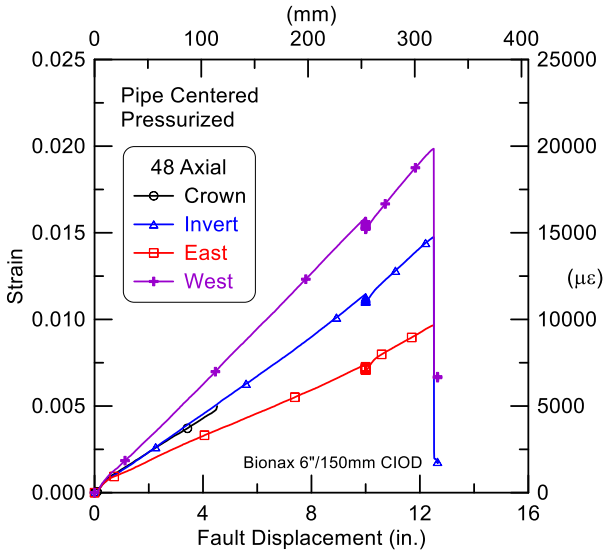

Figure 7.14. Axial Strain vs. Fault Displacement 48 in. (122 cm) North of Fault

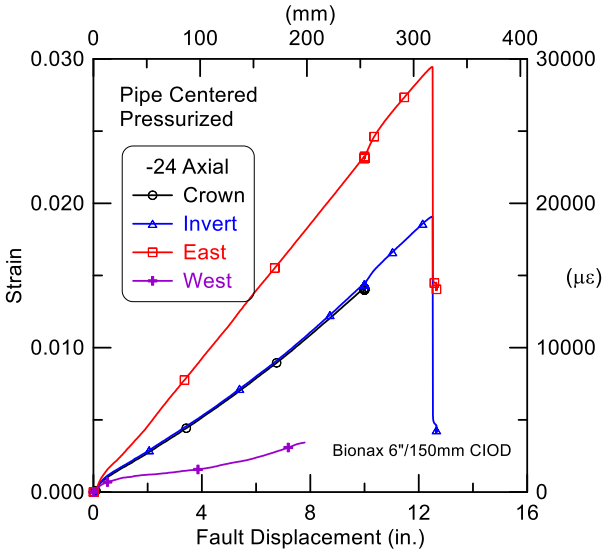

Figure 7.15. Axial Strain vs. Fault Displacement 24 in. (61 cm) South of Fault

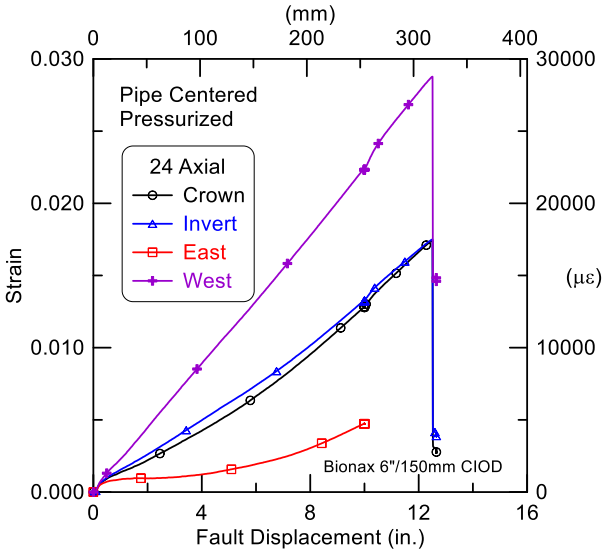

Figure 7.16. Axial Strain vs. Fault Displacement 24 in. (61 cm) North of Fault

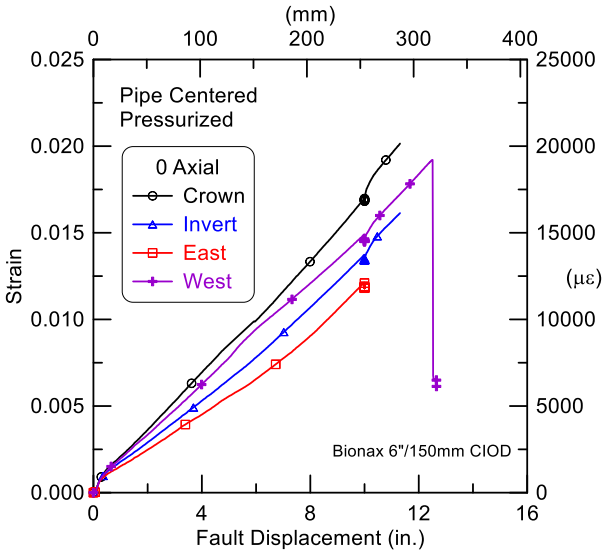

Figure 7.17. Axial Strain vs. Fault Displacement at Fault

The average crown and invert axial strains at all gage locations, both south and north of the fault, are shown in Figures 7.18 and 7.19. The east and west springlines were not included in the averages because in a few cases the east or west springline gage was not functioning and then using only three gages would not represent the axial strains accurately. The progression of strains from far away from the fault increasing to the maximum at the fault is shown clearly in the average axial strain data. The average axial strains are plotted vs. distance from the fault in Figure 7.20. The strains are very symmetric about the fault, and increase as fault displacement increases.

The bending strain, e_b, is calculated as:

$$\varepsilon_b = \frac{\varepsilon_W - \varepsilon_E}{2} \qquad (1)$$

Where ε_E is the measured strain at the gage mounted in the axial direction on the east springline and ε_W is the measured strain at the gage mounted in the axial direction on the west springline. Whether it is (W-E) of (E-W) is somewhat arbitrary. If using this sign convention the direct axial strain on the east side is $\varepsilon_{AE} = \varepsilon_E + \varepsilon_b$ the direct axial strain on the west side is $\varepsilon_{AW} = \varepsilon_W - \varepsilon_b$.

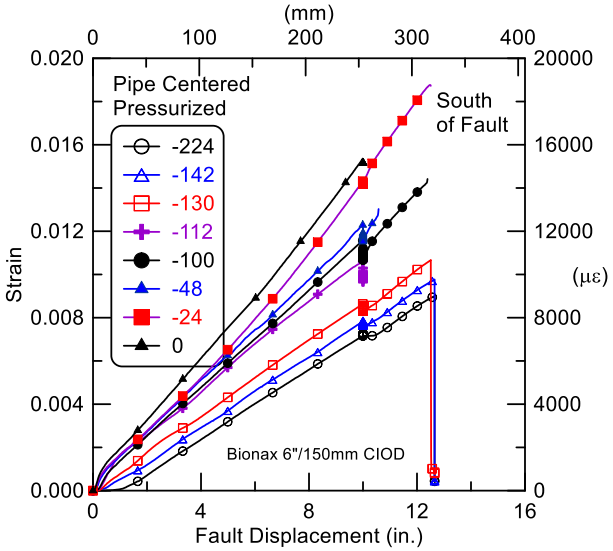

Figure 7.18. Average Crown and Invert Axial Strain vs. Fault Displacement South of Fault

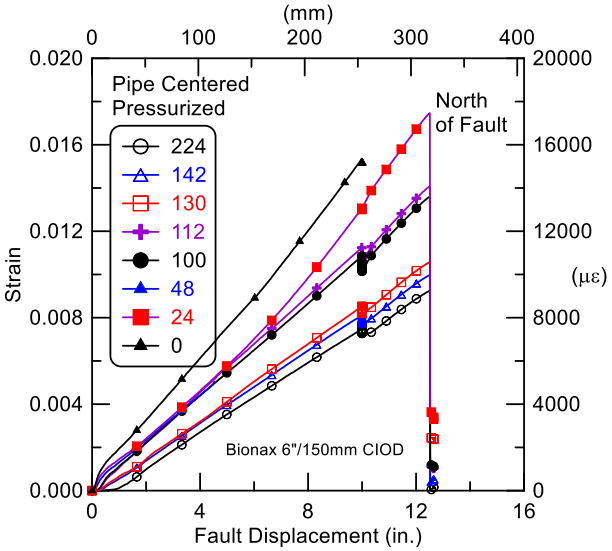

Figure 7.19. Average Crown and Invert Axial Strain vs. Fault Displacement North of Fault

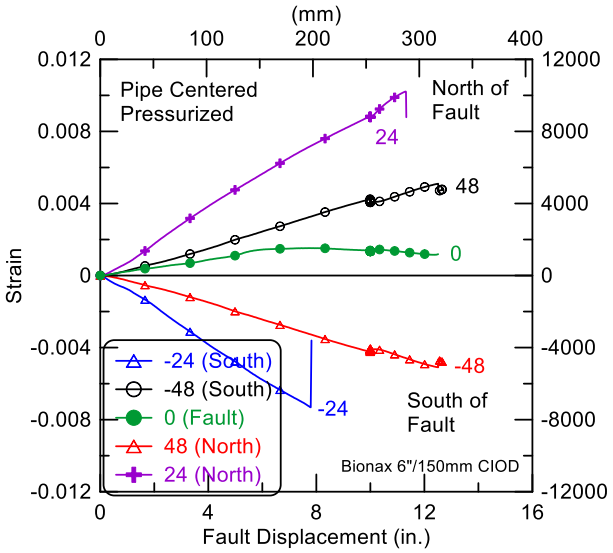

Figure 7.20. Average Crown and Invert Axial Strain vs. Distance from Fault

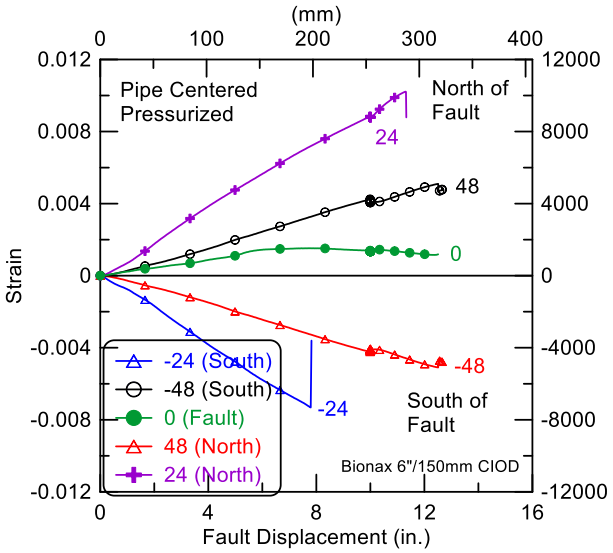

Figure 7.21. Bending Strain vs. Fault Displacement at Fault, 24 in. (61 cm) 48 in. (122 cm) South and North of Fault

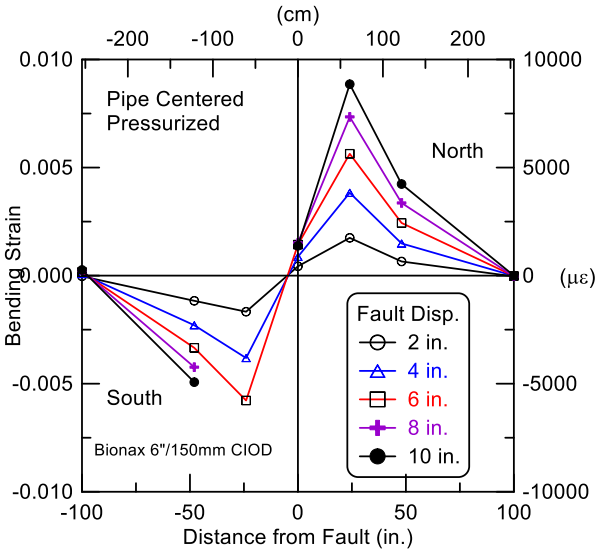

Figure 7.22. Bending Strain vs. Distance from Fault

Figure 7.21 shows the bending strains at the fault (0), 24 in (61 cm) and 48 in. (122 cm) south and north of the fault calculated using Eq. 1. The bending strains are quite symmetric. The bending strain at the fault is relatively small, since this represents the inflection point of the pipe in bending. As previously stated, 100 in. (254 cm) south and north of the fault, the bending strains were near zero. Figure 7.22 shows the distribution of bending strain along the pipeline vs. distance from the fault. The symmetry of the bending strains is quite clear, indicating a symmetric deformed shape with the inflection point at the fault.

8. Joint Movements

The joint movements on the east and west springlines of both the south and north joints are presented in Figure 8.1. The joint movements at the springlines are nearly identical. From roughly 2 in. (51 mm) of fault movement through 10 in. (254 mm) there is a steady increase in the joint openings. At 10 in. (254 mm) the test was paused and the joints still continued to creep open slightly. At a fault displacement of approximately 12.6 in. (320 mm) the pipe near the south joint failed. All joint movements show an abrupt jump in displacement when failure occurred. The joint openings were about 0.6 in, (15.2 mm) at that time. Since there was practically no differential opening on the east and west springlines at both joints, there was no joint rotation at either joint. The absence of joint rotation is consistent with the resistance to rotation provided by the joint restraints.

Figure 8.2 shows the DCDT measurements from the bell side of the joint to the bell side clamp of the restraint and from the bell side to the spigot side clamp of the restraint. In the test pipe, each joint had the bell on the south portion of the joint. So, the bells were facing to the north. The "Bell to Spigot Restraint" (BSR) measurements show that the spigot restraint was being pulled north, consistent with the movement of the test basin to the north along the 50º fault. The "Bell to Bell Restraint" (BBR) measurements indicate that spacing between the bell and bell side restraint decreased. At each joint, the distance between the bell and spigot side restraint increased and the distance between the same location on the bell and the bell side restraint decreased by the nearly the same amount. The small increase in restraint spacing is shown in Figure 8.3. The separation of the clamps increased roughly 0.022 in. (0.56 mm) and 0.015 in. (0.38 mm) across the south and north restraints, respectively, at a fault movement of 12 in. (305 mm).

Figures 8.4 and 8.5 show the average springline movements and the bell to spigot displacements at the south and north joint, respectively. As indicated above, the movements at each joint are nearly the same. In Figures 8.4 and 8.5 the south and north "Bell to Spigot Restraint" (SBSR and NBSR, respectively) are plotted relative to the springline movement (pullout) of the joint. These movements are larger than the SBSR and NBSR movements, indicating that the spigot was pulled through the spigot side clamp at each joint. This pullout was approximately 0.3 in. (7.6 mm) and 0.2 in. (5 mm) for the south and north joint, respectively.

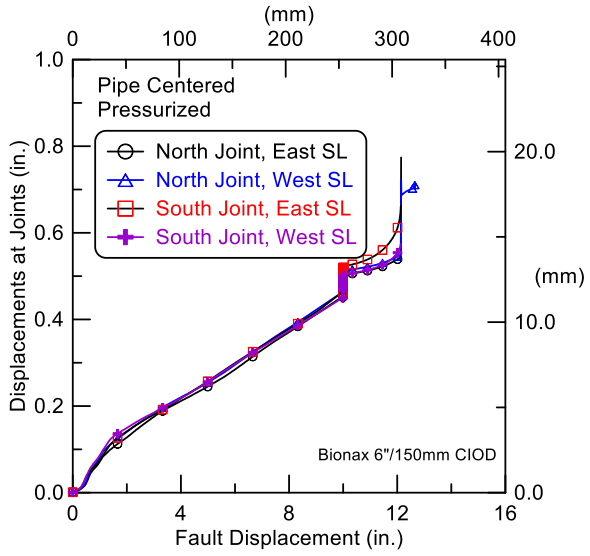

Figure 8.1. Displacements at South and North Joints, East and West Springlines

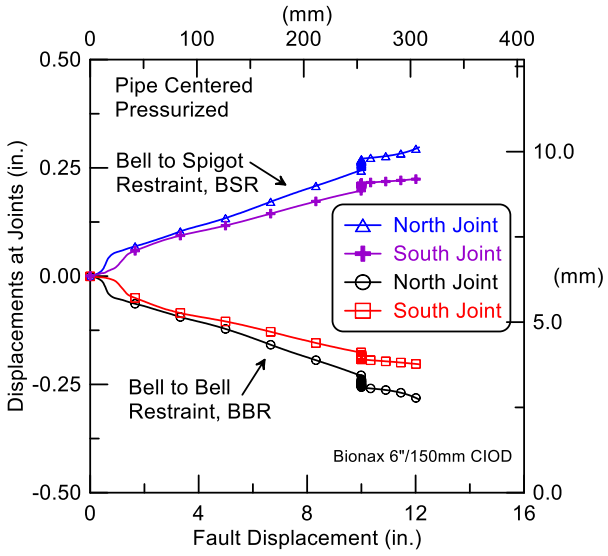

Figure 8.2. DCDT Measurements from Bell End to Bell Restraint and to Spigot Restraint, South and North Joints

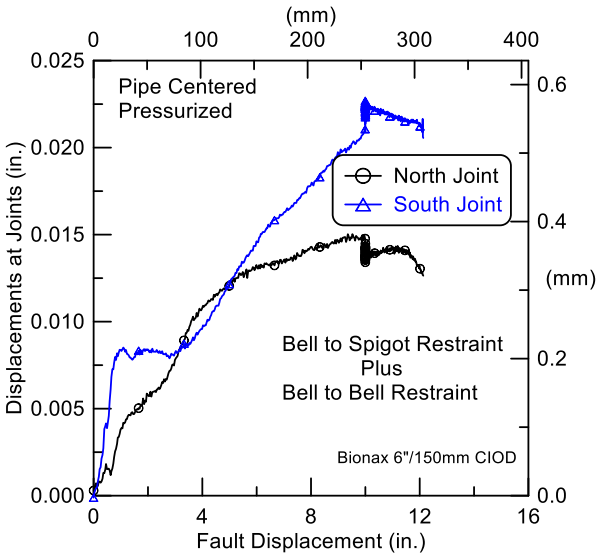

Figure 8.3. Change in Restraint Spacing, South and North Joint

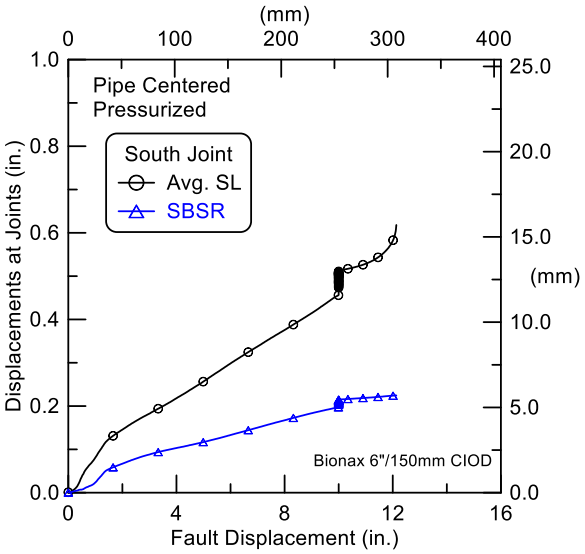

Figure 8.4. South Joint, Average Springline and Bell to Spigot Restraint Displacements

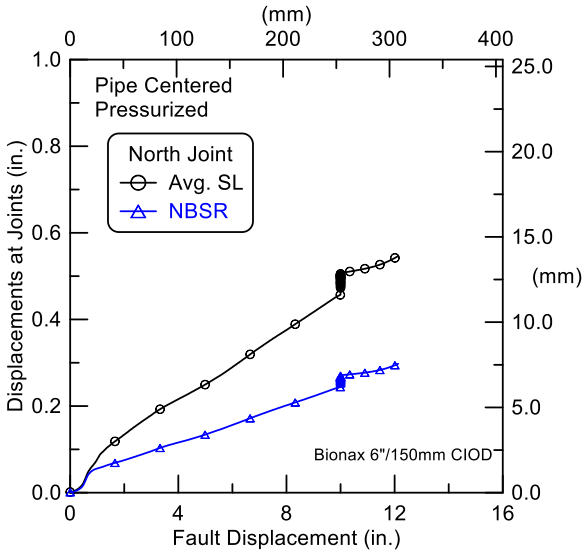

Figure 8.5. North Joint, Average Springline and Bell to Spigot Restraint Displacements

9. Force Measurements

Load cells were placed at the south and north ends of the test basin, outside the ends of the pipe. The load cells measured the forces at four locations between the pipe and structural members of the test basin. Figures 9.1 and 9.2 show the four load cell measurements at the south and north ends, respectively, of the test basin. The greatest variation in load cell measurement was registered at the south end. Figure 9.3 shows the summation of all four load cells at each end of the test basin. The total loads at the ends are in reasonable agreement, in the range of 16 to 18 kips (71 to 80 kN).

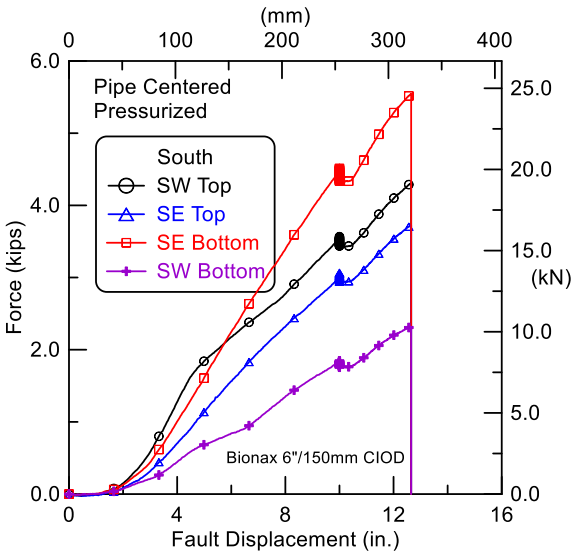

Figure 9.1. South End Load Cells

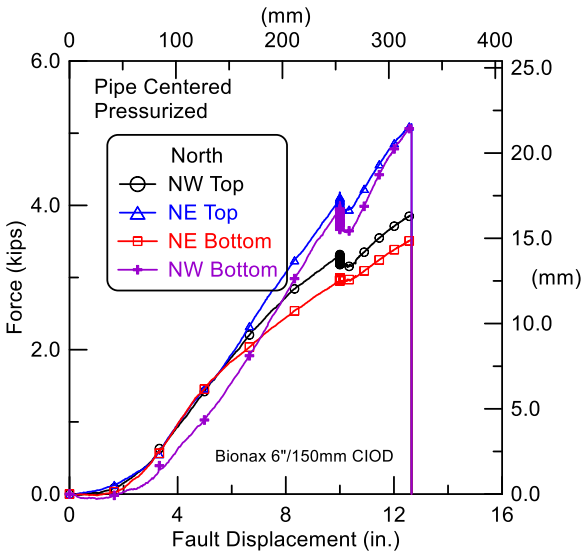

Figure 9.2. North End Load Cells

The strain gages at plane -224 on the south end and 224 on the north end are outside the soil, and 18 in. (45.7 cm) from the inside end of the test basin. The outside diameter of the pipe was OD = 6.9 in. (175.3 mm) and the average measured wall thickness of t_w = 0.245 in. (6.22 mm). This gives a pipe wall cross-sectional area of A = 5.12 in.^{2} (3304.7 mm^2). The average Young's modulus of the Bionax in the linear range of the stress vs. strain relationship is E = 437 ksi (3.01 GPa). This was determined from several tensile coupon tests, and previously reported to IPEX ("Task 1 - Material Testing of Bionax Pipe and Joints," Cornell University, Sep. 2013). Using the average crown and invert strains at these two gage planes and multiplying the strain times AE gives the force in the pipe. Figures 9.4 and 9.5 show the forces in the south and north pipe sections at the -224 and 224 gage planes, respectively, calculated using the pipe strains with the force measured by the four load cells at each end. The linear strain-based forces are consistently higher than the summation of the four load cells at both the south and north ends. If the effects of initial load cell adjustments, thrust from internal pressure on the test pipe end caps, and nonlinear stress vs strain effects are accounted for, the forces calculated from the strain gages at the time of pipe failure are in agreement with the load cell measurements.

The distribution of axial force along the pipe, again calculated for a linear relationship between stress vs. strain as axial force, $F = \varepsilon AE$, is shown in Figure 9.6. There is increasing axial force with larger fault displacement, resulting in a maximum force of 40 kips (180 kN) at the fault crossing (0 distance). If a nonlinear analysis for the relationship between stress vs. strain is used, the maximum axial force at the fault crossing is approximately 33 kips. The reduction in force occurs because the axial strains at the fault crossing require less strain for mobilization when nonlinear stress response is accounted for.

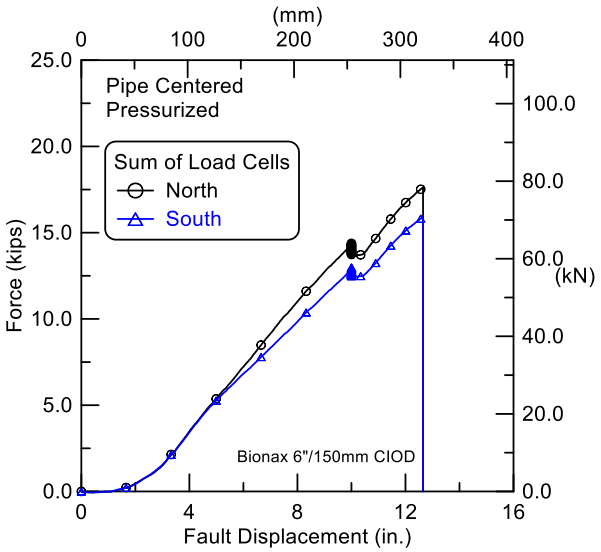

Figure 9.3. Sum of All Load Cells, South and North Ends

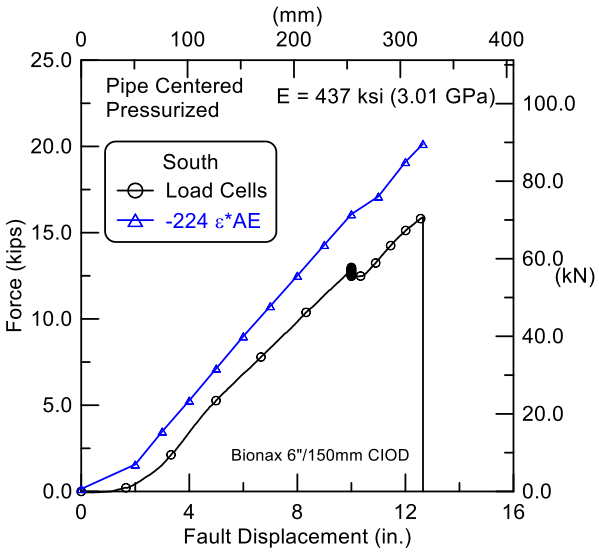

Figure 9.4. South Load Cells and Strain Gage Force vs. Fault Displacement

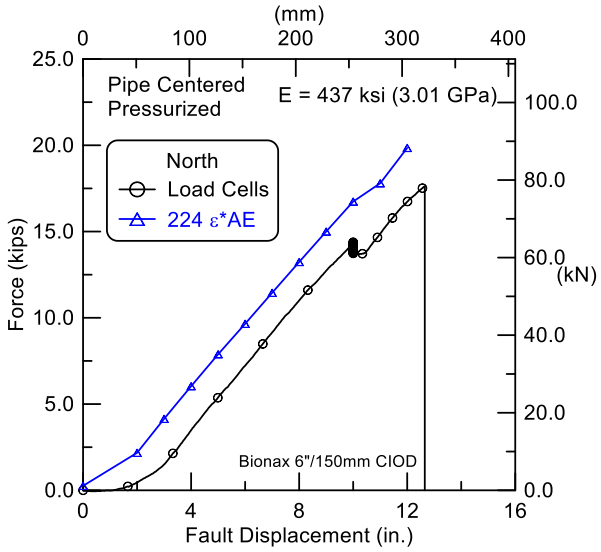

Figure 9.5. North Load Cells and Strain Gage Force vs. Fault Displacement

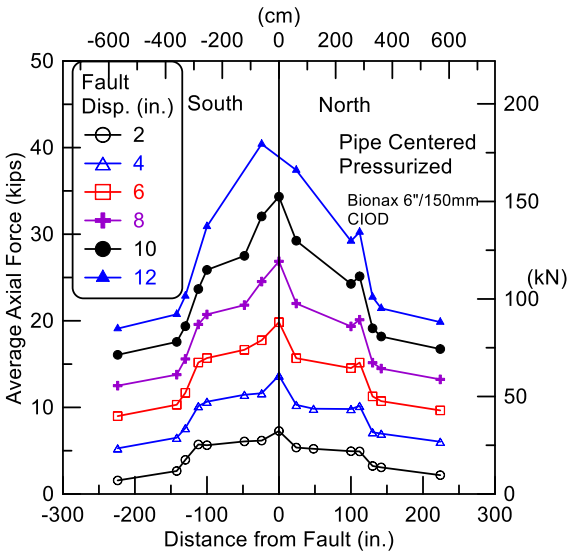

Figure 9.6. Axial Force in Pipe vs. Distance from Fault

10. Summary

A 40-ft (12.2-m)-long, three-piece section of a Bionax 6 in. (150mm) CIOD pipeline was tested at the Cornell Large-Scale Lifelines Facility. The pipe had two joints, equally spaced about a 50º fault. The joints were fitted with UFR1559-C-6-I restraints for C909 PVCO. The pipe was instrumented with seventy-two strain gages installed in fifteen locations along the pipeline to measure strains and to evaluate axial forces and bending moments. Strain gages were positioned at the crown (C), invert (I) east (E) springline, and west (W) springline of the pipe. There were four DCDTs at each joint to measure joint and restraint movements and to evaluate joint rotation. Four load cells were placed outside the pipe basin at each end, reacting between the test basin structural frame and pipe end restraint to measure axial force. The pipe was pressurized to approximately 80 psi (552 kPa).

The pipe was placed on a bed of compacted sand, aligned, instruments checked, and then backfilled with compacted sand to a depth of cover of 30 in. (762 mm) above the pipe crown. The test basin's north section was displaced along a 50º fault at a rate of 2 in. (51 mm) per minute. The basin was displaced roughly 10 in. (254 mm), paused, and then put in motion again. At a fault displacement of roughly 12.6 in. (320 mm) there was an audible "pop," the pipe lost pressure, and the test was stopped. The 12.6 in. (320 mm) fault displacement corresponds to 8.1 in. (206 mm) of axial extension of the test basin and pipe. Following excavation, a full circumferential fracture of the pipe was observed just beyond the northern most restraint at the south joint.

Figure 10.1 shows the fault rupture at pipe failure. Figure 10.2 shows the deformed pipe partially excavated following the test along with the rupture at the south joint. Figure 10.3 is a close-up photo of the south joint along with the protective DCDT covering, and the ruptured pipe.

The maximum axial strain in the pipe developed at the fault crossing. At the maximum fault movement the axial strain at the pipe center was roughly 1.8%. The strains increased smoothly as the fault was displaced from 0 to 12.6 in. (0 to 320 mm). The bending strains were localized within 100 in. (254 mm) either side of the fault. Bending strains were near zero at the fault (inflection point) and largest (roughly 1%) at a distance of 24 in. (61 cm) south and north of the fault.

The end forces at the south and north end of the test basing were on the order of 16 to 18 kips (71 to 80 kN). The axial force in the pipe, as determined from the strain gage readings for an assumed linear relationship between stress vs. strain, was largest at the fault crossing, and would be roughly 40 kips (180 kN). If the nonlinear relationship between stress vs. strain is used, the maximum axial force at the fault crossing is approximately 33 kips.

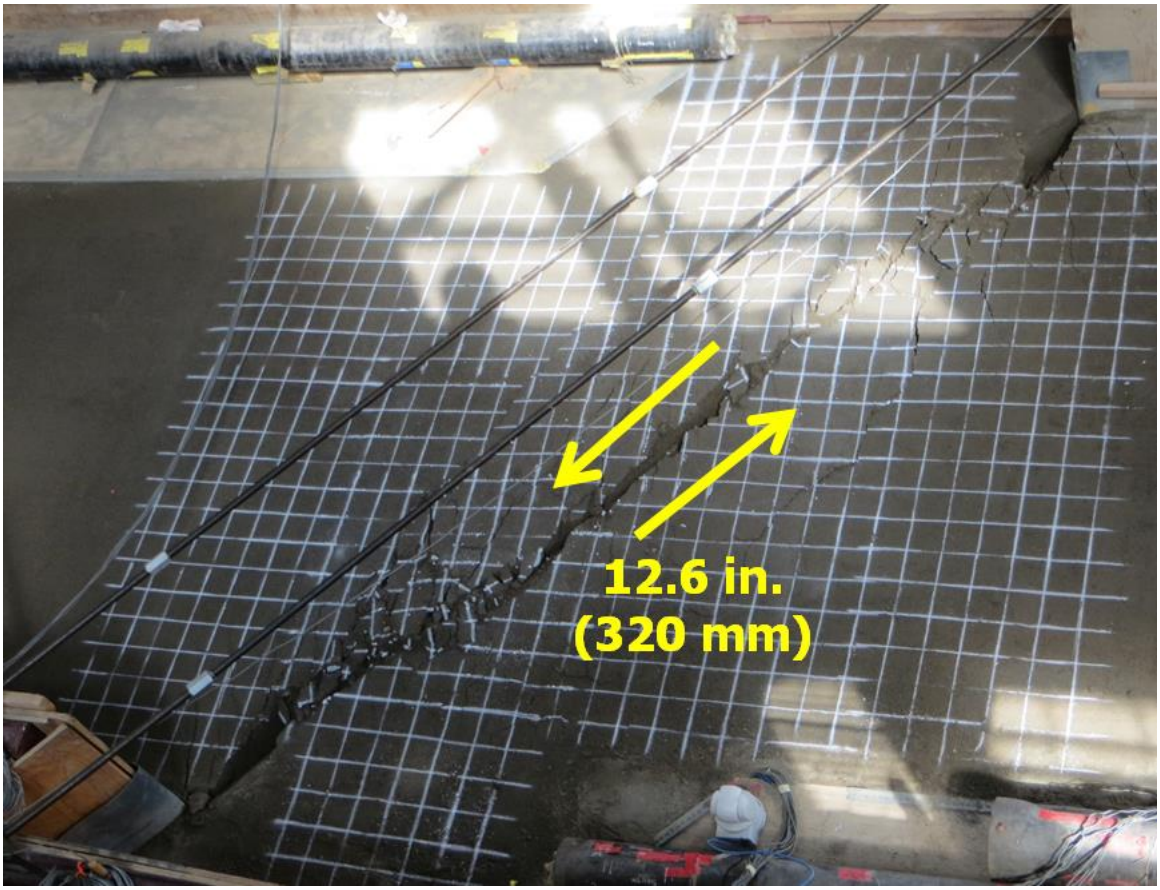

Figure 10.1. Fault Rupture at Pipe Failure

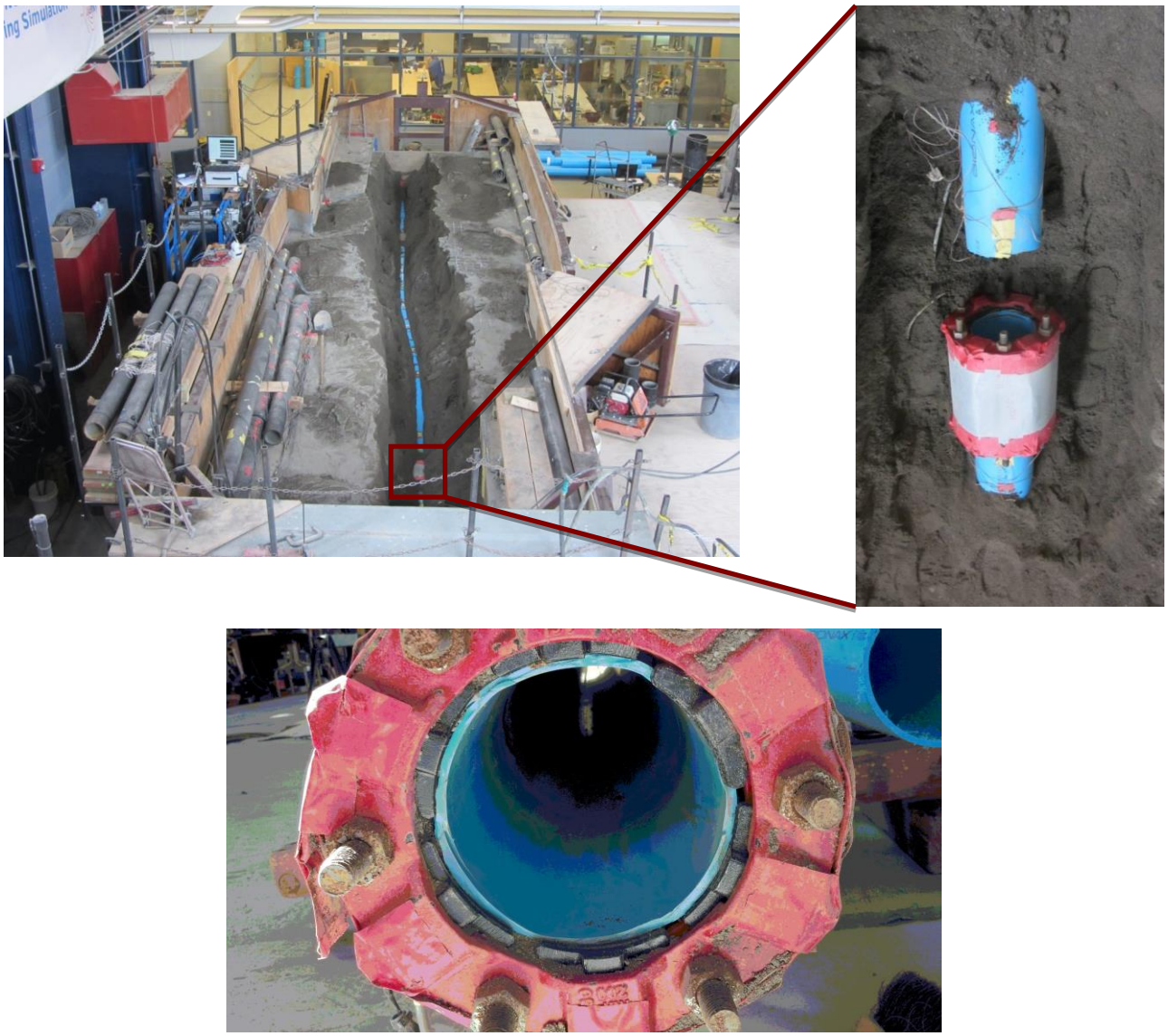

Figure 10.3. South Joint after Excavation

The restrained pipeline was able to accommodate significant fault movement through axial tensile and bending strains in the pipe in combination with some axial slip at the restrained joints. The fault rupture simulated in the large-scale test is also representative of the most severe ground deformation that occurs along the margins of liquefaction-induced lateral spreads and landslides.

Overall the pipeline was able to accommodate 8.1 in. (206 mm) of axial extension, corresponding to an average tensile strain of 1.67% along the pipeline. Such extension is large enough to accommodate the great majority of liquefaction-induced lateral ground strains measured by high resolution LiDAR after each of four major earthquakes during the recent Canterbury Earthquake Sequence in Christchurch, NZ (O'Rourke, et al., 2013).

Further improvements in pipeline performance are possible through relatively simple modification of the restraint. Such modification would allow axial slip at the joints before bolt engagement and transmission of force to the collars of the restraint. A similar adjustment could be made to accommodate compression. The modification provides for initial axial slip before additional axial elongation or compression of the pipe develops in conjunction with increasing axial forces at the joints. It is estimated that the axial strain accommodated by the pipeline could be increased by 50 to 100% by this relatively simple modification.

A similar large-scale split box test on a ductile iron pipeline with push-on joints was conducted at Cornell. The test involved a ductile iron (DI) pipe specimen with 6 in. (150 mm) nominal diameter. The DI pipe joint consisted of a standard bell and spigot connection sealed with a greased Tyton® rubber gasket. The general layout of the test was similar to the IPEX test described in this report. The pipe consisted of three DI sections within soil, with additional pipe sections added to make the total pipe length sufficiently long to exit the test basin. The three central pipe sections in soil were 9, 12, and 9 ft (2.74, 3.66, and 2.74 m) long. The central 12-ft (3.66-m)-long section was centered on the 50º fault. This is referred to as the "pipe centered" condition. The same compacted glacio-fluvial sand was used as in the IPEX test, with a depth of cover above the pipe crown of 30 in. (762 mm.) The average soil dry unit weight was 106.8 lb/ft^3 (16.8 kN/m^3) and the average moisture content was 4.3%.

The pipe was pressurized to 75 psi (517 kPa) prior to any basin movement. Leakage during the test occurred when the spigot end pulled from the bell at the joint on the south side of the fault rupture, similar in location to the failed IPEX joint. The fault displacement of the ductile iron pipe at joint pull out was approximately 5.5 in. (140 mm). This corresponds to an axial movement of 3.5 in. (89 mm) [fault movement · cos 50º]. When leakage occurred the opening at the south joint was 2.4 in. (61 mm) and at the north joint 1.1 in. (28 mm).

References

O'Rourke, T.D., Jeon, S-S., Toprak, S., Cubrinovski, M., Jeon, J.K. (2012) "Underground Lifeline System Performance during the Canterbury Earthquake Sequence", *Proceedings*, Invited Keynote Paper, 15th World Conference on Earthquake Engineering, Lisbon, Portugal, 24p.

"Task 1 - Material Testing of Bionax Pipe and Joints," Cornell University, Sep. 2013.

Appendix A – Instrumentation Locations

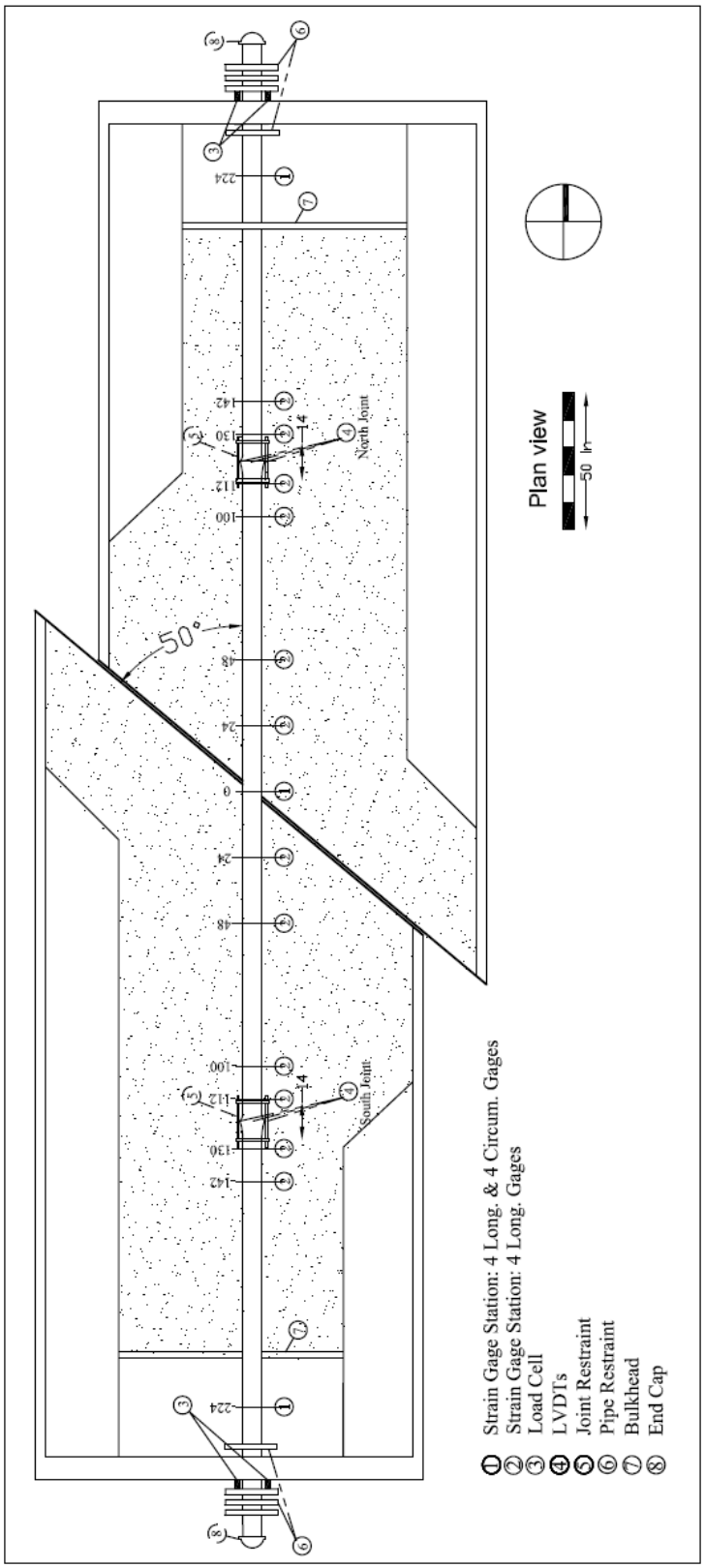

Figure A.1. Expanded Instrumentation Layout

Appendix B – Additional Photos

Figure B.1. Instrumented Pipe in Test Basin Prior to Backfill

Figure B.2. Pipe after Test Showing South Joint

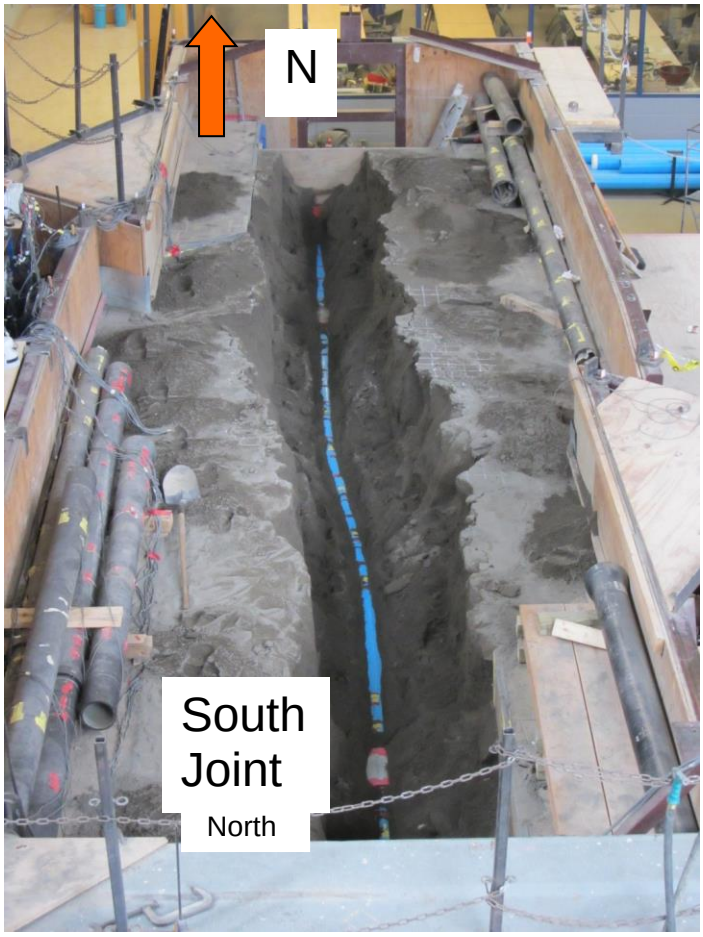

Figure B.3. Overview of Pipe in Basin after Test

Figure B.4. South Joint after Pipe Rupture

a) Pipe Side

b) Restraint Side

B.6. Ruptured Pipe at South Restraint

Figure B.7. South Joint Showing Ruptured Pipe and Joint Protective Enclosure

Figure B.8. South Joint Showing Ruptured Pipe

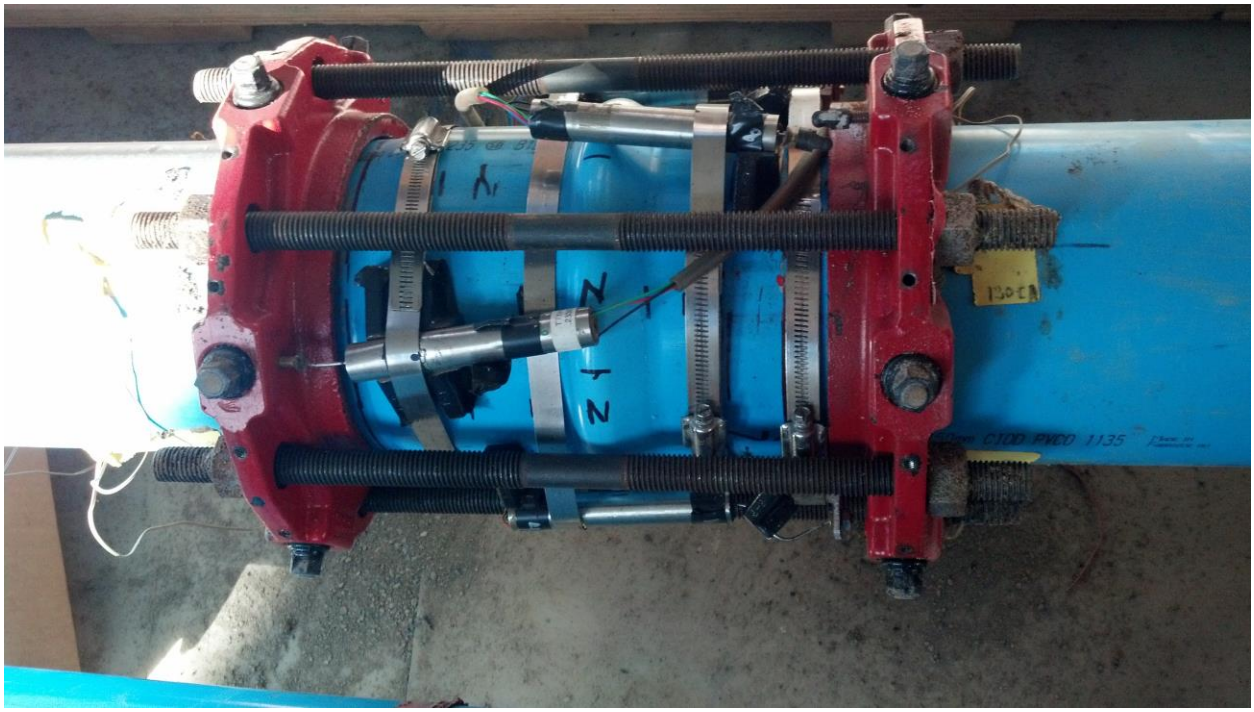

Figure B.9. North Joint after Test with Protective Enclosure Removed